Ceramics International 47 (2021) 27420–27429

Contents lists available at ScienceDirect

Ceramics International

journal homepage: www.elsevier.com/locate/ceramint

Model on thermal conductivity prediction of quasi-columnar structured coating by plasma spray physical vapor deposition

Shi-Yi Qiu [a,b], Jia Shi [a], Shan Li [a], Chen-Wu Wu [b,*], Chen-Guang Huang [b], Yue Ma [a,**], Hong-Bo Guo [a]

[a] School of Materials Science and Engineering, Beijing Key Laboratory for Advanced Functional Material and Thin Film Technology, Beihang University BUAA, Beijing, 100191, PR China

[b] Institute of Mechanics, Chinese Academy of Sciences, Beijing, 100190, China

ARTICLE INFO

Keywords:
Thermal conductivity
Quasi-columnar structured coating
Plasma spray physical vapor deposition (PS-PVD)
Thermal barrier coating (TBC)
Thermodynamic model

ABSTRACT

Firstly, the yttria-stabilized zirconia (YSZ) coating and gadolinium zirconate (GZO) coating with the quasi-columnar structure were manufactured by plasma spray physical vapor deposition. At the same time, a novel three-dimensional geometrical model was established that could satisfactorily reflect such quasi-columnar structural characteristics. Then, based on this model, the three-dimensional spatial distribution of pores and porosity of coatings and the thermal resistance behaviors of the quasi-columnar structured coating were analyzed. Later on, the thermodynamic model was established to estimate the thermal conductivity of the quasi-columnar structured coatings at different temperatures. Finally, a model for predicting the effective thermal conductivity of the GZO/YSZ double-layer coating with quasi-columnar structure was validated to account for the effects of the variable thickness ratios of GZO top layer to YSZ inner layer.

1. Introduction

Nowadays, thermal barrier coating (TBC) is essential for aero and land-based gas turbine engines to decrease the temperature of metallic substrates and prolong the lifetime of components in hot sections of gas turbines [1–3]. Generally, the thermal barrier coating system consists of a ceramic coat used for thermal insulation and a bonding coat used for relieving thermal mismatch between ceramic coat and metallic substrate [4]. The ceramic coat with different microstructures and properties can be obtained by adopting different processes. Typically, the two main methods for coating preparation are atmospheric plasma spray (APS) and electron beam physical vapor deposition (EB-PVD). The APS coating has a typical lamellar structure formed by the solidification of liquid droplets. This coating has great thermal insulation performance but poor thermal shock resistance [5–7]. The EB-PVD coating has the columnar structure formed by the deposition of vapor-phase atoms. This coating has excellent strain tolerance for thermal shock but has poor thermal insulation performance due to the lack of transverse interface in coating [8–10].

In recent years, a novel coating preparation technology, plasma spray physical vapor deposition (PS-PVD), has emerged. This coating technology simultaneously takes advantage of atmospheric plasma spray and electron beam physical vapor deposition methods and fills the gap between these methods [11–15]. In the preparation process, the system can pump the chamber down to extremely low pressure of 100 Pa and equipped with a super high power (up to 180 kW) spraying torch. Also, the plasma jet can extend more than 2 m in length and up to 0.4 m in diameter [16–18]. Thus, coating with different microstructures, including dense lamellar structure, EB-PVD-like columnar structure, and quasi-columnar structure [19], can be made at different spray distances. Note that the quasi-columnar structured coating is formed by co-deposition of vapor phases, liquid droplets, and solid particles. Also, this coating retains the columnar structure and has good strain tolerance for thermal shock. At the same time, the quasi-columnar structure is formed by stacking the small columns, which is equivalent to create many interfaces between small columns in the coating. Thus, the interfaces may greatly enhance the thermal insulation performance of the coating [20].

In some studies, the quasi-columnar structure coatings were manufactured by PS-PVD, and their thermophysical and mechanical

* Corresponding author.
** Corresponding author.
E-mail addresses: chenwuwu@imech.ac.cn, c.w.wu@outlook.com (C.-W. Wu), mayue@buaa.edu.cn (Y. Ma).

https://doi.org/10.1016/j.ceramint.2021.06.164
Received 24 May 2021; Received in revised form 16 June 2021; Accepted 19 June 2021
Available online 20 June 2021

properties were analyzed. Also, the yttria-stabilized zirconia (YSZ), a common material used for thermal barrier coatings, was chosen to study PS-PVD coating. For example, Gao [15] manufactured the YSZ quasi-columnar structured coating by PS-PVD and investigated coatings' thermal conductivity and thermal cycling behavior. The results showed that the YSZ coating with quasi-columnar structure had a lifetime of 2000 cycles during the thermal cycling test, while exhibiting relatively low thermal conductivity. Zhang [20] prepared the YSZ quasi-columnar structured coating by PS-PVD co-deposition of vapor phases, liquid phases, and solid particles. Zhang developed the three-dimensional deposition model of quasi-columnar structured coating and revealed the formation mechanisms of the quasi-columnar structured coating. At present, with developing the knowledge of PS-PVD technology, new materials have been used to prepare PS-PVD coatings. Note that the gadolinium zirconate ($Gd_2Zr_2O_7$, GZO), with extremely low thermal conductivity [22], is a potential candidate for thermal barrier coating. Li [23] successfully developed a kind of GZO particles that can be used in PS-PVD through sintering the particles in special craftsmanship. Li obtained a GZO quasi-columnar structured coating at a suitable spraying distance of PS-PVD. Zhu [24] fabricated GZO single-ceramic-layer (SCL) coating and GZO/YSZ double-ceramic-layer (DCL) coating with quasi-columnar structure by PS-PVD. Zhu carried out the water-quenching experiments on the coatings, and the results showed that the GZO/YSZ DCL coating has a better thermal shock resistance than the GZO SCL coating.

However, the reason for the effective thermal resistance of the quasi-columnar structured coating has not been revealed yet because there are few studies on the thermophysical properties of the quasi-columnar structure coating. Since experimental observation of the heat flow conduction in the structure is not easy, a thermodynamic model is an appropriate method to investigate thermophysical properties of the quasi-columnar structured coating. Thus, a coating model can be used to simulate the conduction process of heat flow in the coating structure and to study the heat resistance mechanism of the quasi-columnar structure. At the same time, the thickness of the PS-PVD ceramic layer used in actual engineering is between 100 and 200 μm, which is too thin to peel off into a free-standing coating to measure the thermal conductivity accurately. Thus, it is important to develop a thermal conductivity prediction model for quasi-columnar structured coatings by PS-PVD.

In this paper, the YSZ and GZO coatings with the quasi-columnar structure were manufactured using plasma spray physical vapor deposition equipment. Based on the deposition mechanism and the observed structural characteristics of the quasi-columnar structured coating, a novel method is proposed to establish three-dimensional quasi-columnar structured coating models of the YSZ and GZO coatings. It will be shown that this model can satisfactorily reflect the quasi-columnar structural characteristics. Then, through the spatial topology calculation, the pores in the coating are extracted, and the three-dimensional spatial distribution of pores and porosity are analyzed. Note that the results of calculated porosity are equivalent to the experimental results of coating samples. The thermal conduction process of the coating is simulated by the finite element method, and the thermal resistance mechanism of the quasi-columnar structured coating is analyzed. Then, the thermal conductivity prediction model is established to estimate the thermal conductivity of YSZ and GZO coatings at different temperatures. It will be shown that the predicted results are in good agreement with experimental data of coating samples. Finally, for the GZO/YSZ double-layer coating, commonly used in engineering, an effective thermal conductivity prediction model for GZO/YSZ double-layer quasi-columnar structured coating is developed. This model can predict the effective thermal conductivity of coatings with different thickness ratios of the GZO top layer to the YSZ inner layer.

2. Description of experiments

2.1. Coating preparation

The YSZ and GZO coatings with the quasi-columnar structure were prepared by PS-PVD equipment (Medicoat, AG, Switzerland). The PS-PVD system is equipped with an MC-100 plasma torch with a power capability of up to 120 kW and a vacuum pump unit that could pump the chamber down to a low working pressure of 100 Pa. The feedstock of the YSZ coating was Metco6700 8 wt% yttria partially stabilized zirconia powder, while the feedstock of the GZO coating was the sintered $Gd_2Zr_2O_7$ (GZO) powder. Note that the details of GZO powders preparation can be found in our previous work [23]. For thermal conductivity measurement, to gain the free-standing coating, the coatings were directly sprayed on a graphite substrate of 12.7 mm in diameter and 3 mm in thickness. Note that the spraying parameters of YSZ and GZO coatings are shown in Table 1. Then, the graphite substrate was removed by polishing to obtain the free-standing coating. The porosity of the coating was estimated by the image analysis method. Note that the polished cross-section of the coating was observed by a scanning electron microscope, and a number of microscopic structure images were randomly selected. According to the threshold method, the image analysis software Image J was adopted to perform black-and-white binarization on the cross-section images of the coating to separate the pores from the coating. The porosity of each image was calculated, and the average value and the standard deviation were computed. The results showed that the porosity of YSZ coating was 35.5% ± 1.5%, and that of GZO coating was 29.3% ± 0.9%.

2.2. Measuring thermal conductivity

The thermal conductivity of coatings was calculated by Eq. (1):

$$\kappa = \phi \times C_p \times \rho, \tag{1}$$

First, the thermal diffusivity (ϕ) was measured by the laser flash method [25] in the utilization of FLA427 equipment. The graphite was sprayed on the upper surface of the sample for laser absorption and heat conduction. The sample's upper surface was irradiated by a pulsed laser beam, and the temperature of the sample's lower surface was monitored at each moment. Then, the time when the temperature of the lower surface reached half of the maximum temperature was recorded. This time was used to calculate the thermal diffusivity by Eq. (2) [25]:

$$\alpha = 0.1388\frac{L^2}{t_{\frac{1}{2}}}. \tag{2}$$

The specific heat capacity (C_p) of YSZ and GZO could be calculated using the heat capacity of the component oxides based on the Neumann-Kopprule rule [26–28]. The specific heat capacity of YSZ and GZO were calculated by the following formula for several temperature levels as listed in Table 2 and Table 3, respectively. The actual density (ρ) of the coating was calculated with the porosity and theoretical density. Note that the density of YSZ and GZO coatings was 3.805 and 4.894 g/cm^3, respectively (see Table 4).

$$C_{p-YSZ} = 0.08C_{p-Y_2O_3} + 0.92C_{p-ZrO_2} \tag{3}$$

$$C_{p-GZO} = 0.595C_{p-Gd_2O_3} + 0.405C_{p-ZrO_2} \tag{4}$$

2.3. Microstructure analysis

Fig. 1 shows the microstructure of the coatings observed by the Quanta 200F scanning electron microscope. Fig. 1(a)–(d) show the microstructure of YSZ coating and Fig. 1(e)–(h) show the microstructure of the GZO coating. As shown in Fig. 1(a), (b), (e), and (f), both YSZ and GZO coatings exhibit a typical quasi-columnar structure. The coating

Table 1
Spraying parameters of YSZ and GZO coatings.

Coaitng	Gun power (KW)	Current(A)	Ar(slpm)	He(slpm)	Distance(mm)	Carrier gas(slpm)	Feed rate(g·min-1)
YSZ	65	2000	30	60	1000	10	~6
GZO	60	2000	30	60	1000	11	~4

Table 2
Theoretical specific heat capacity of YSZ.

Temperature (°C)	200	400	600	800	1000	1200
Cp-8YSZ(J/(g K))	0.541	0.578	0.600	0.616	0.631	0.644

Table 3
Theoretical specific heat capacity of GZO.

Temperature (°C)	400	600	800	1000	1200
Cp-GZO(J/(g K))	0.434	0.448	0.461	0.472	0.483

Table 4
The porosity of coating models.

Coating Model	*Vp* (μm^3)	*Vc* (μm^3)	*p*
YSZ	256529.27	494721.03	34.14%
GZO	352853.2864	863146.714	29.01%

consists of coarse columns composed of many small island-like columns stacked on each other. This implies that, within a coarse column, there are lots of interfaces and voids between the small columns, as shown in Fig. 1(c), (d), (g), and (h). Compared with the columnar structured coatings prepared by EB-PVD, such microstructure coating has many transverse interfaces and gaps within a coarse column, which may greatly improve the thermal insulation performance of the coating.

3. Modeling

According to the PS-PVD deposition mechanism [20,21,29], the quasi-columnar structured coating is formed by co-deposition of vapor phases, liquid droplets, and solid particles. Initially, the gas-phase atoms nucleate non-uniformly on the surface of the substrate and then continuously absorb the vapor-phase atoms to grow and form small island-shaped columns. However, when the small island-shaped column continues to grow, the solid or liquid particles in the flame flow arrive at the surface of the island-shaped columns, which will interrupt the columns' growth. This is because these particles on the columns' surface will become new nucleation centers, where gas-phase atoms will re-nucleate and grow into new island-shaped columns. In such a deposition process, the coating forms the microstructural characteristic of a coarse column. This coarse column is composed of a number of small island-shaped columns stacked on each other. Fig. 1 obviously shows this stacking in the microstructural graph of the coating. At the same time, many interfaces and obvious gaps are formed between the small columns due to stacking small island-shaped columns.

The distribution of small island-shaped columns and the inter-column voids in the coarse columns can be found by observing the polished cross-sectional morphologies of the coating. A statistical method is adopted to reconstruct the two-dimensional distribution of small island-shaped columns in coatings. Then, a three-dimensional structure model will be established based on the two-dimensional distribution of the structure. This three-dimensional model can satisfactorily reflect the typical microstructural characteristic of the quasi-columnar coating and the three-dimensional distribution of the pores in coatings.

To establish the three-dimensional model, firstly, several SEM micrographs of the polished cross-section of the coating were randomly selected. Then, the distribution of each small island-shaped column in the coating was reconstructed manually in the photographs, in which the island-shaped column was drawn approximately in the shape of an ellipse. Thus, the actual shape and size of each small column were reflected. Note that, in the process of manual reconstruction, the gaps between small columns were deliberately retained to best mimic the real situation. Also, in each microphotograph, a structure with a width of 100 μm was randomly selected for reconstruction, and four two-dimensional distribution graphs of each coating were obtained. Then, the three-dimensional modeling was performed on each small column in the two-dimensional distribution graph, and four groups of three-dimensional structural units with a width of 100 μm of each coating were obtained.

Finally, four groups of three-dimensional structural units were arranged one behind the other to generate a structure square matrix, and

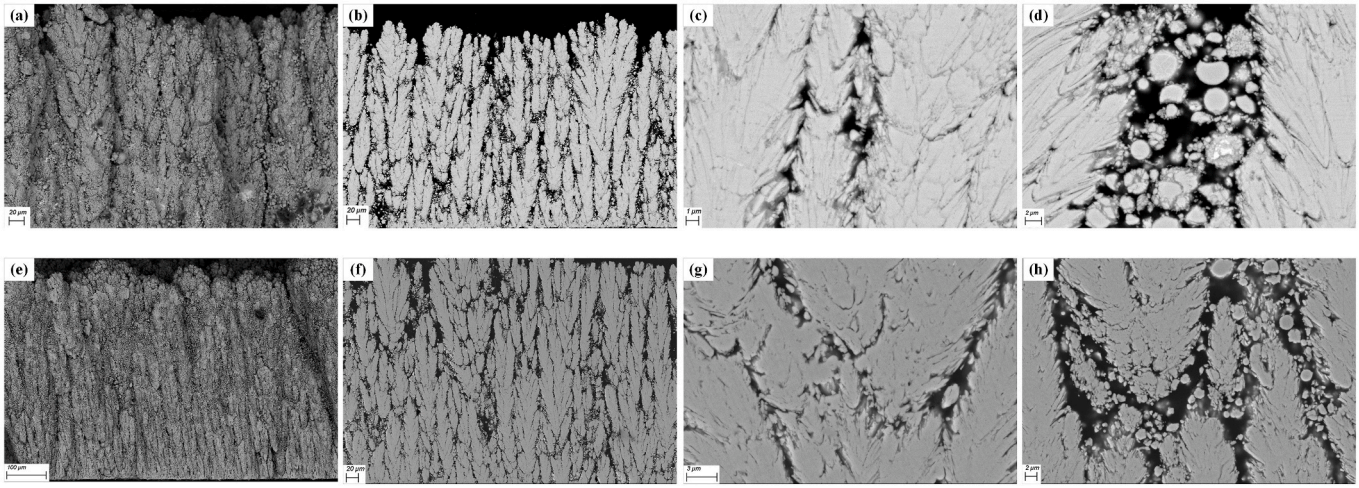

Fig. 1. The SEM micrograph of the PS-PVD coatings, (a) fractured cross-section, (b) polished cross-section, (c) and (d) voids and interfaces between small columns of the YSZ coating, (e) fractured cross-section, (f) polished cross-section, (g) and (h) voids and interfaces between small columns of the GZO coating.

the quasi-columnar microstructure coating model was established. Note that the height of the YSZ coating model is 320 μm, and the height of the GZO coating model is 410 μm. The YSZ and GZO modeling processes are shown in Figs. 2 and 3, respectively.

The quasi-columnar structured coating model is shown in Fig. 4, in which the YSZ and GZO coating models are compared with the microscopic fractured cross-section of coating samples. It can be seen that the coating model well reflects the typical quasi-columnar structural feature of coarse columns consisting of multiple small island-shaped columns. Also, the cross-sections of the coating model at different depths were obtained and compared with the polished cross-sectional micrographs of the coating samples. The results show similar distributions of the voids, which also proves that the model can satisfactorily reflect the real distribution of the voids in the quasi-columnar structured coating.

4. Analysis of coating porosity

The pores between the columns in the coating model can be extracted using computer graphics and geometric topology operations [30,31]. These pores can be used to analyze the three-dimensional distribution of pores and to calculate the porosity of coatings. The three-dimensional object in the space exists in the form of a bounded set in the n-dimensional Euclidean space (E^n). This three-dimensional object is expressed as G = {bG, iG}, where bG is the (n-1) dimensional boundary of the set, and iG is the interior of the set. The set of coating part is expressed as G_c, the set of pores is expressed as G_p, and the union set of coating and pores is expressed as G_w. According to the derivation of computational geometry, to obtain the set of pores, it is necessary to perform a difference operation in space, as shown in the following formulas:

$$G_w = G_C \cup G_p, \tag{5}$$

$$G_p = G_w - G_C. \tag{6}$$

In computer graphics [32], the difference operation will be rearranged as shown in Eq. (7). The detailed steps are the intersection detection, intersection, classification and merging.

$$G_p = G_w - G_w \cap G_C. \tag{7}$$

The most important step is the intersection operation, for which the key step is calculating intersection boundary lines of the intersection of surfaces between the entities. Note that the intersecting surfaces are set as:

$$P_1 : \ \overrightarrow{n_1} \cdot P = s_1, \tag{8}$$

$$P_2 : \ \overrightarrow{n_2} \cdot P = s_2. \tag{9}$$

Note that the direction of the intersecting lines is expressed as $\overrightarrow{n_1} \times \overrightarrow{n_2}$. The point set on the intersection lines is expressed as:

$$\mathrm{P} = \mathrm{a}\overrightarrow{n_1} + b\overrightarrow{n_2}. \tag{10}$$

The points of set also exist on both surfaces s_1 and s_2, and the values of parameters a and b can be obtained by solving the plane equation as:

$$\mathrm{a} = \frac{s_2\overrightarrow{n_1}\cdot\overrightarrow{n_2} - s_1||\overrightarrow{n_2}||^2}{(\overrightarrow{n_1}\cdot\overrightarrow{n_2})^2 - ||\overrightarrow{n_1}||^2||\overrightarrow{n_2}||^2}, \tag{11}$$

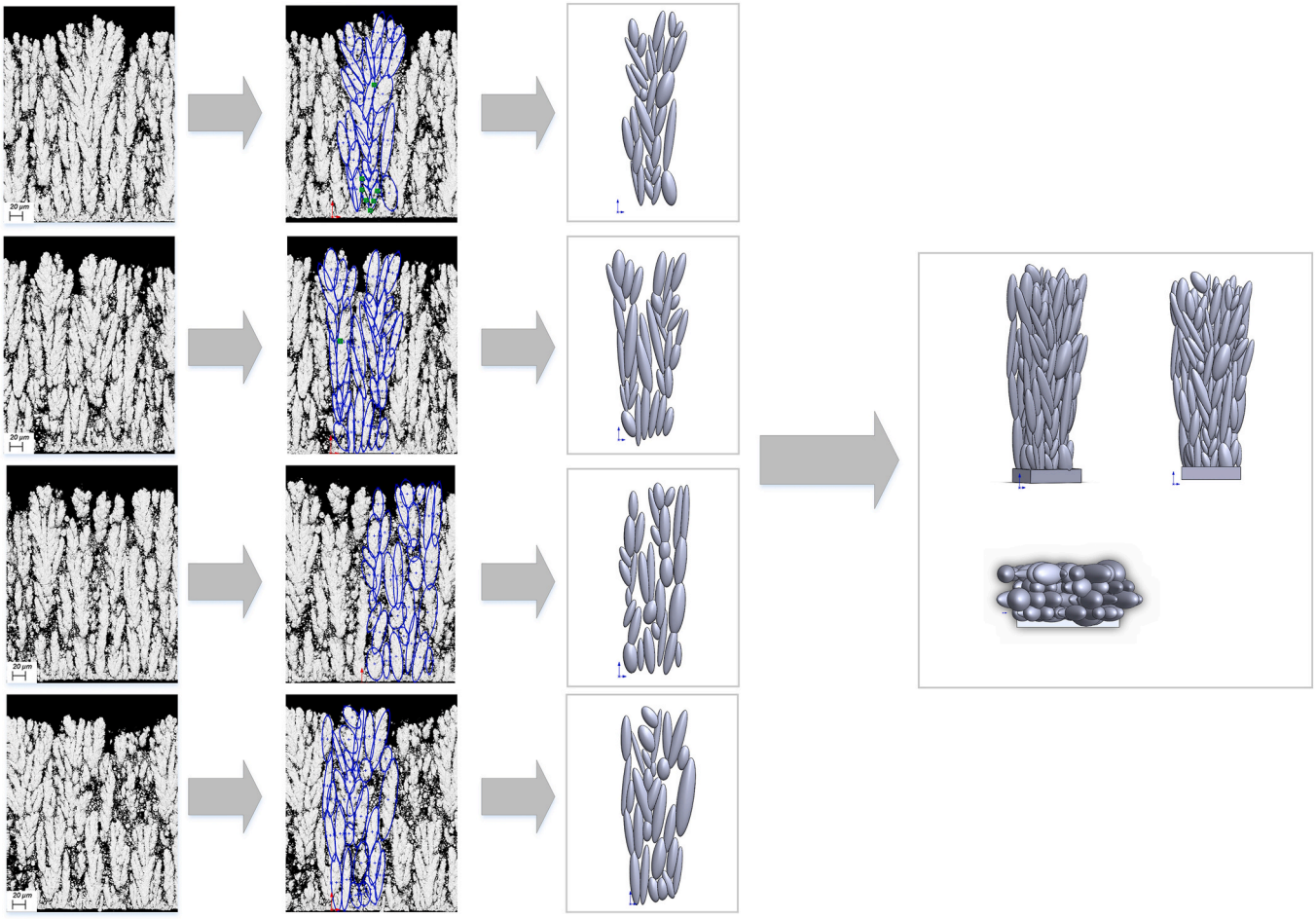

Fig. 2. The process of YSZ coating modeling.

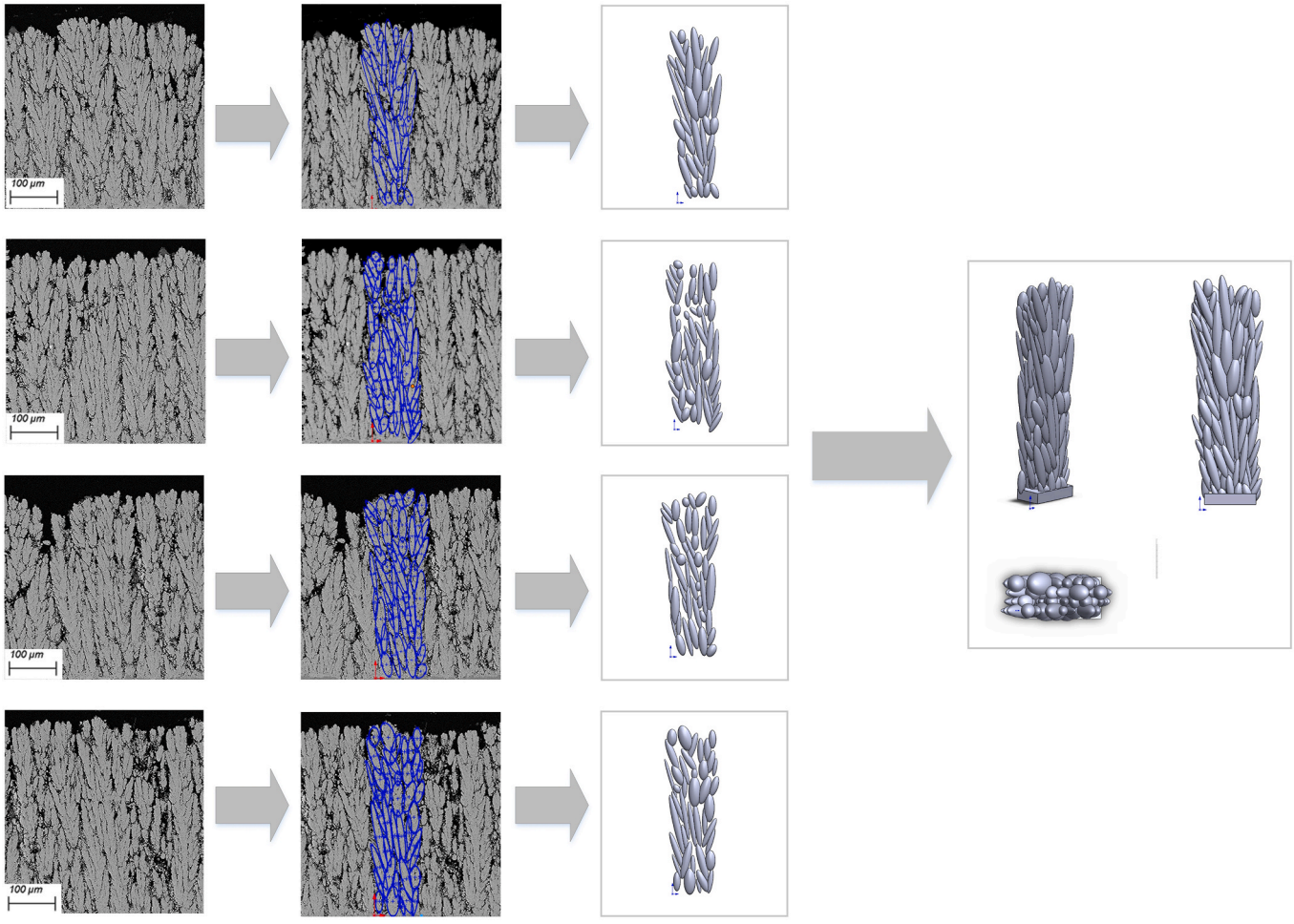

Fig. 3. The process of GZO coating modeling.

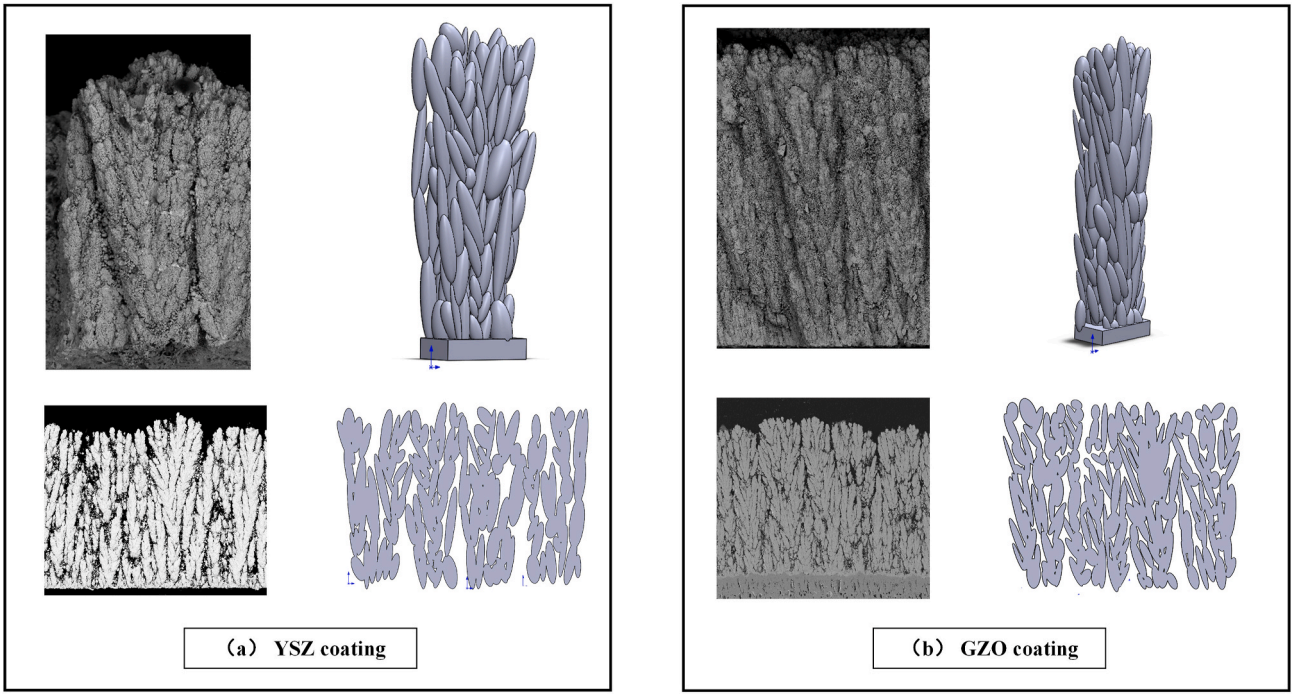

Fig. 4. Comparison of three-dimensional coating models and coating samples, (a) the YSZ coating model and (b) the GZO coating model.

$$b = \frac{s_2\overrightarrow{n_1}\cdot\overrightarrow{n_2} - s_2||\overrightarrow{n_1}||^2}{(\overrightarrow{n_1}\cdot\overrightarrow{n_2})^2 - ||\overrightarrow{n_1}||^2||\overrightarrow{n_2}||^2}. \quad (12)$$

Finally, the function of intersecting line is attained as:

$$L = P + t(\overrightarrow{n_1} \times \overrightarrow{n_2}) = (a\overrightarrow{n_1} + b\overrightarrow{n_2}) + t(\overrightarrow{n_1} \times \overrightarrow{n_2}). \quad (13)$$

Note that the boundary lines between the coating and pore parts are attained by multiple intersection operations. Then, the part of $G_w \cap G_C$ in the set G_w is removed through the classification judgment algorithm. Finally, the set of pore parts is obtained, which is expressed as $G_p = \{bG_p, iG_p\}$. The three-dimensional visualization results of pores part are shown in Fig. 5.

After extracting the inter-column pores in the quasi-columnar structured coating, the porosity of the coating can be calculated by Eq. (14). The porosity results of the YSZ and GZO coating models are shown in Table 2. The porosity of the YSZ coating model is 34.14%, which is close to the experimental measurement value (35.5% ± 1.5%) of the YSZ coating sample. Also, the porosity of the GZO coating model is 29.01%, which is almost equal to the experimental measurement value (29.3% ± 0.9%) of the GZO coating sample.

$$p = \frac{V_p}{V_p + V_c}, \quad (14)$$

where *Vp* is the volume of the pore part, and *Vc* is the volume of the coating part.

Next, the pore distribution of the columnar coating is studied. The porosity of the top and bottom areas of the YSZ and GZO coating models are calculated. The results show that in the YSZ quasi-columnar structure coating, the porosities of the top and bottom areas are 39.5 and 31.3%, respectively. In contrast, in the GZO quasi-columnar structure coating, the porosities of the top and bottom areas are 32.5 and 24.6%, respectively. Note that, in the two quasi-columnar structured coatings, the inter-column pores are inter-connected, and the porosity of the top area is more than the bottom area.

5. Analysis of coating heat conduction behavior

The heat conduction process of the quasi-columnar structure coating is simulated by calculating the temperature field using the finite element method. Constant temperatures of *T*1 and *T*2 (*T*1 > *T*2) are assumed on the top and bottom of the model, respectively, and the rest of surfaces are set as adiabatic, as shown in Fig. 6. Note that the finite element model of the YSZ coating has a total of 127219 nodes and 564,598 elements. The finite element model of GZO coating has a total of 430,996 nodes and 2038714 elements. The geometric model, finite element model, and temperature field of the quasi-columnar structured coating model are shown in Fig. 7.

The heat flux fields of the YSZ and GZO coating models are respectively shown in Fig. 8(a) and (c), in which it can be observed that the heat flux at the interface between the small column is extremely large. Fig. 8(b) and (d) are the two-dimensional cross-sectional graphs of the heat flux field of the YSZ and GZO coating models, respectively. Note that a trend graph of the heat flux is drawn with a path (red line in the figure), which is taken on the cross-sectional view. Then, the heat flux on the path is recorded. The results show that when the heat flux passes through an interface between small columns, the heat flux will increase sharply. Also, in the steady-state heat conduction, the greater the heat flux is, the smaller the effective contact area is. As can be seen in Eqs. (15) and (16), a larger thermal resistance of the structure is generally achieved by decreasing the effective contact area. The results indicate that, in the quasi-columnar structured coating, the stack of small

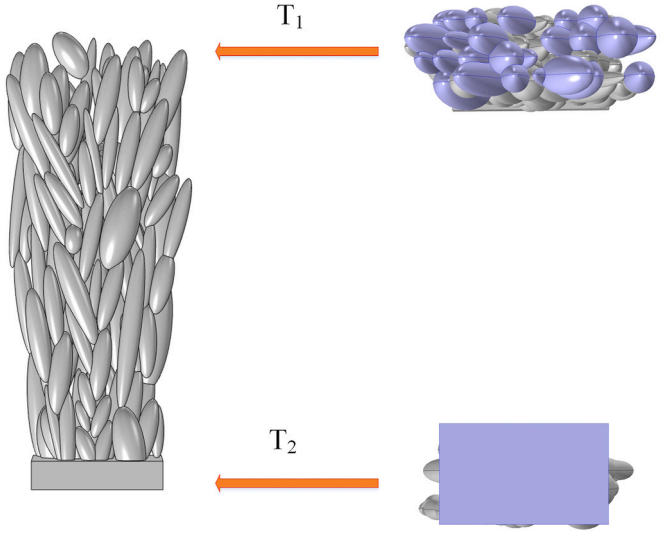

Fig. 6. The diagram of the boundary conditions of the quasi-columnar structured coating model.

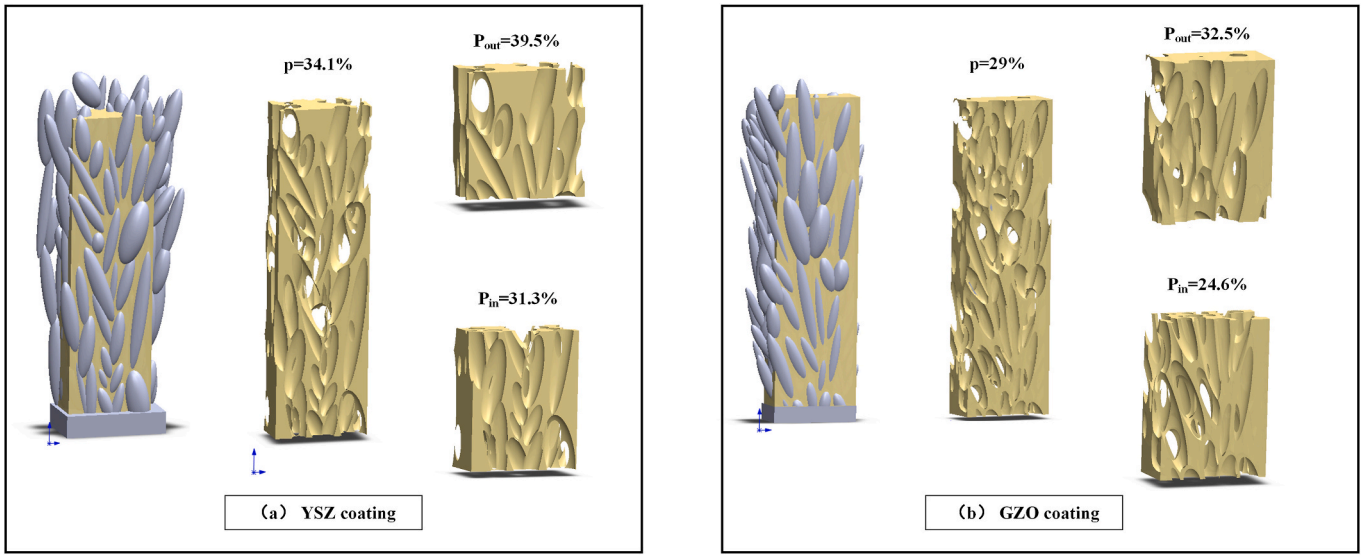

Fig. 5. The three-dimensional visualization results of pores in coatings, (a) the YSZ coating, and (b) the GZO coating.

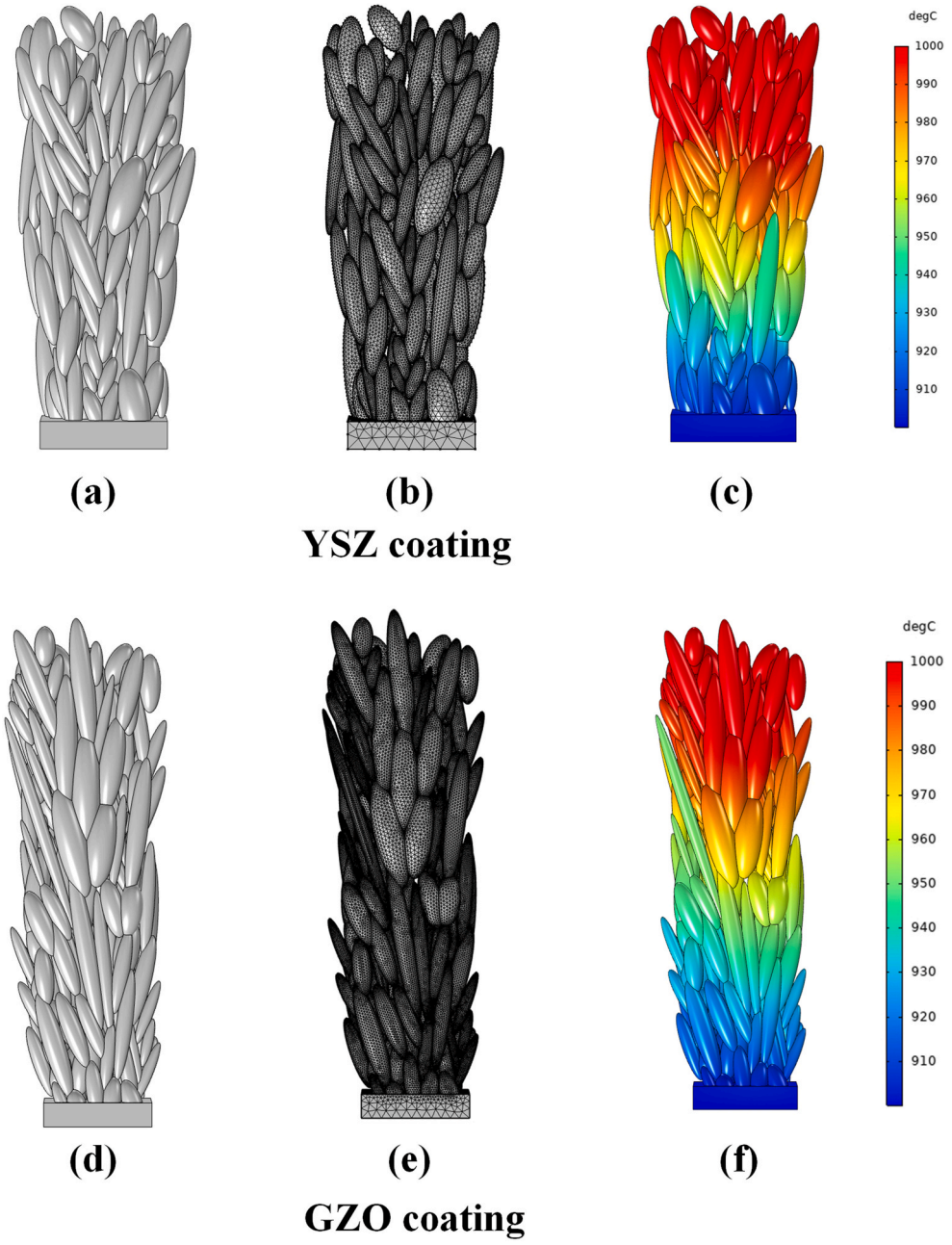

Fig. 7. The YSZ coating model: (a) geometric model, (b) meshed finite element model, and (c) temperature contours, and the GZO coating model: (d) geometric model, (e) meshed finite element model, and (f) temperature contours.

columns forms a large number of interfaces between small columns with a small effective contact area, which greatly increases the thermal resistance of the coating structure. Thus, the quasi-columnar structured coating exhibits great thermal resistance property.

$$\mathrm{Q} = \mathrm{k}\frac{\Delta T}{\mathrm{h}}A, \tag{15}$$

$$R = \frac{\Delta T}{Q} = \frac{h}{kA}. \tag{16}$$

6. Prediction model of thermal conductivity

To estimate the effective thermal conductivity of quasi-columnar structured coating at different temperatures, the temperature field needs to be calculated using the finite element method. The calculation of thermal conductivity is based on the thermal conductive differential equation and Fourier's Law:

$$\rho C_p \frac{\partial T}{\partial t} = k\nabla^2 T, \tag{17}$$

$$q = -k\nabla T, \tag{18}$$

where C_p is the specific heat capacity, ρ is density, k is thermal conductivity, and q is heat flux vector.

Note that the thermal conduction simulation of the quasi-columnar structure coating is based on steady-state heat conduction. Thus, the time-derivative term in Eq. (17) needs to be set to zero. Since the thermal resistance along the thickness is desired, the effective thermal conductivity in the y-direction is calculated as:

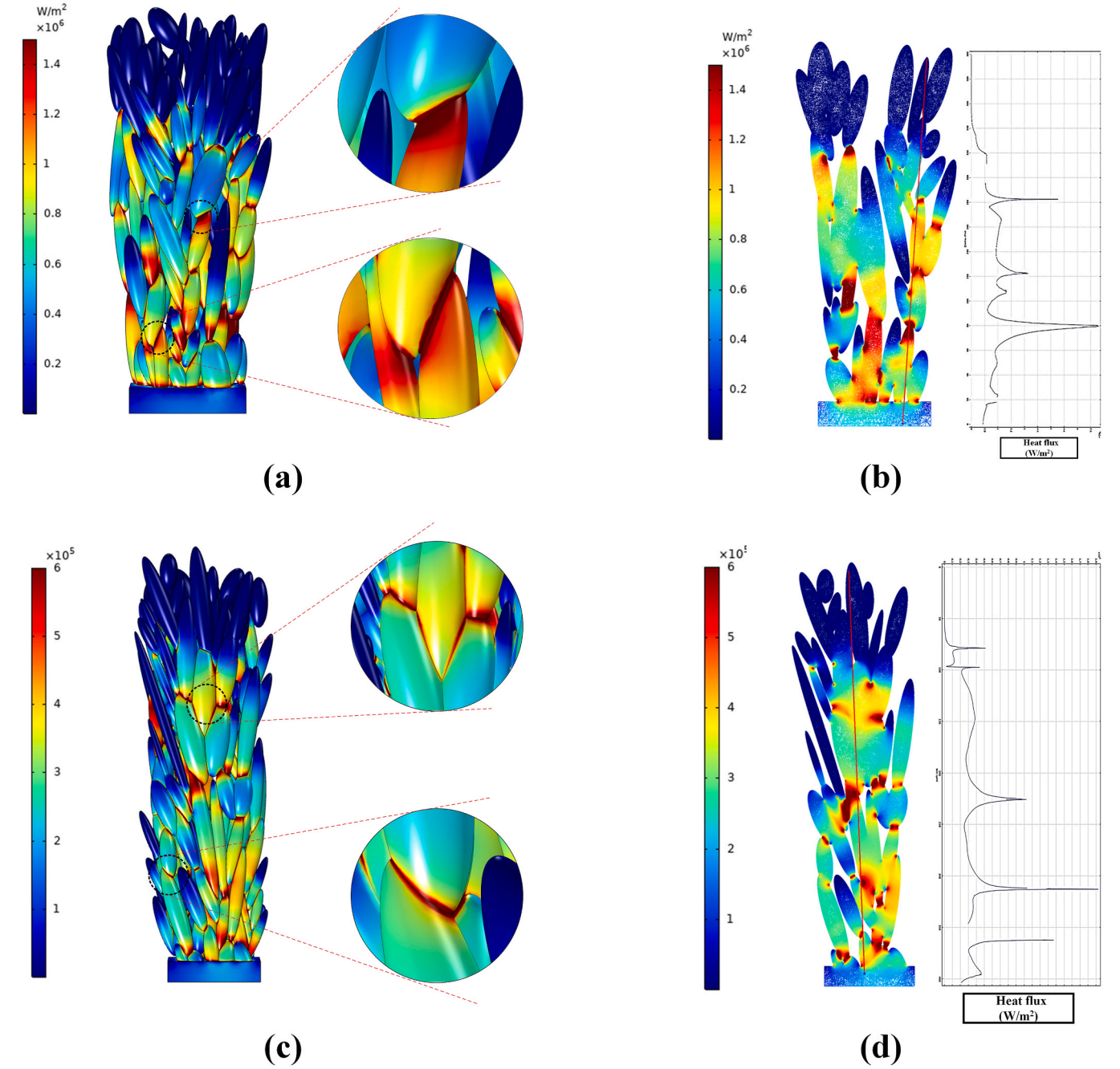

Fig. 8. The YSZ coating model: (a) heat flux field, (b) cross-section of heat flux field, the GZO coating model: (c) heat flux field, (d) cross-section of heat flux field.

$$k_{eff} = \frac{qh}{T_1 - T_2}, \tag{19}$$

where T_1 is the temperature at the top of the coating, T_2 is the temperature at the bottom of the coating, and h is the coating thickness.

Finally, in finite element model, the heat flux q of the bottom surface of the coating at each temperature is attained, and the effective thermal conductivity at each temperature is calculated using Eq. (19). The predicted results of effective thermal conductivity at different temperatures are shown in Fig. 9. As seen, the predicted results of the YSZ and GZO coating models are in good agreement with the experimental data.

In recent years, the design of GZO/YSZ double-layer columnar structured coating has been extensively studied and applied in practical engineering [24,33,34]. Note that the GZO top layer has excellent thermal resistance performance and phase stability. Also, the YSZ inner layer can resolve the issue of low coefficient of thermal expansion and low fracture toughness of GZO. The thermal resistance of double-layer coating depends on the ratio of the thickness of the GZO top layer to the YSZ inner layer. The influence of the thickness ratio of the double layers on the thermal conductivity of GZO/YSZ double-layer coatings prepared by suspension plasma spray have been analyzed in different experiments, e.g., Refs. [35,36]. However, the thermal conductivity of double-layer quasi-columnar coating by PS-PVD has not been sufficiently studied. Thereby, it is necessary to develop a double-layer quasi-columnar coating model to predict the thermal conductivity of the GZO/YSZ double-layer coating with different thickness ratios to save experimental cost and provide a theoretical reference for the design of double-layer quasi-columnar TBCs by PS-PVD.

Based on the previous investigation of the YSZ and GZO coating models, the thermal conductivity prediction model of the GZO/YSZ

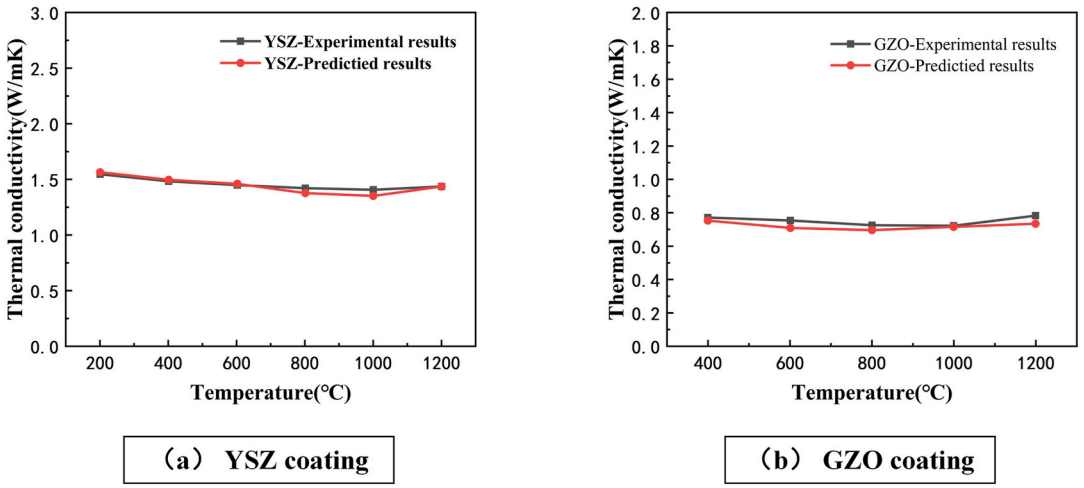

Fig. 9. Comparison of numerical and experimental results, (a) YSZ coating, (b) GZO coating.

double-layer quasi-columnar coatings is designed, as shown in Fig. 10. The thermal conductivity of the double-layer coatings with different thickness ratios at different temperatures is calculated. The ratios of the thickness of the GZO top layer to the YSZ inner layer are 150/150, 200/150, 250/150, and 300 μm/150 μm. Fig. 11 shows the numerical results of the effective thermal conductivity of double-layer coatings with different thickness ratios of GZO/YSZ layers. Note that Fig. 11 can also be used to analyze the effects of variable thickness ratios of the GZO/YSZ layer on the thermal conductivity of the coating. The results indicate that the increase of thickness of GZO top layer with a constant thickness of YSZ inner layer will lead to the decrease of thermal conductivity of the GZO/YSZ double-layer quasi-columnar structured coating.

7. Conclusion

This paper proposed a novel method to establish a three-dimensional quasi-columnar structured coating model, based on the deposition mechanism and microstructure characteristics of the quasi-columnar structured coating by PS-PVD. Note that the coating model could satisfactorily reconstruct the quasi-columnar structural characteristic of the coating. Also, the YSZ and GZO and GZO/YSZ double-layer coating models were established.

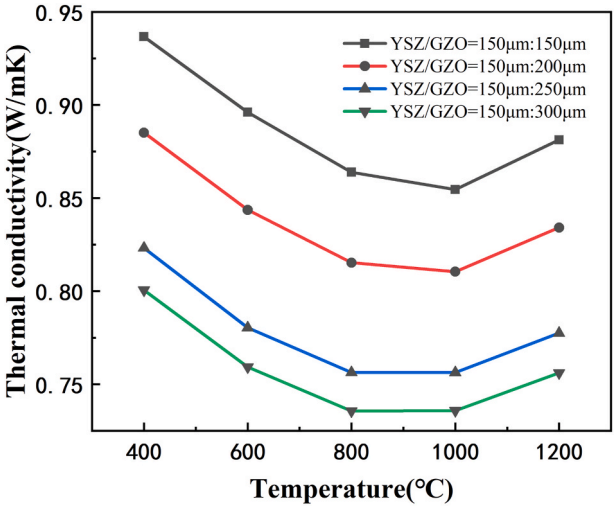

Fig. 11. The effective thermal conductivity of double-layer coating models with different thickness ratios of GZO/YSZ layers.

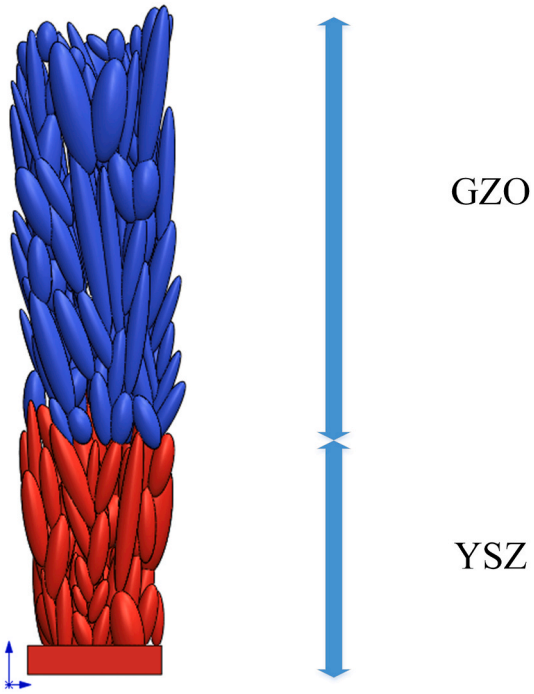

Fig. 10. The GZO/YSZ double-layer quasi-columnar coating model.

The pores in the quasi-columnar structured coating were extracted by the spatial topology calculation to analyze the three-dimensional spatial distribution of pores. It was found that the inter-column pores are interconnected.

In addition, the porosity of the coating models was calculated. Note that the calculated results are very close to the experimental data. The porosity of different parts of the coating was calculated separately, and the results revealed that the porosity of the top of the coating is greater than that of the bottom of the coating.

The heat conduction process of the quasi-columnar structure coating was simulated by the finite element method. The analysis of the heat flux field revealed that there is a large structural thermal resistance at the interface between the small columns. The large thermal resistance of quasi-columnar structure is due to the presence of many interfaces between small columns in the coating. Therefore, the coating exhibits good thermal resistance performance.

The thermal conductivity prediction models of the YSZ and GZO coatings with the quasi-columnar structure were established. Also, the

effective thermal conductivity of the YSZ and GZO coatings at each temperature was calculated. The results were in good agreement with the experimental data. Finally, a GZO/YSZ double-layer quasi-columnar coating model was developed. This model, at different temperatures, could predict the effective thermal conductivity of the double-layer coating with different ratios of the GZO top layer thickness to the YSZ inner layer thickness.

Note that the quasi-columnar structured coating models can also be used for simulation and investigation of the mechanical behavior of PS-PVD coatings in future studies.

Declaration of competing interest

The authors declare that they have no known competing financial interests or personal relationships that could have appeared to influence the work reported in this paper.

Acknowledgments

This research is supported by the National Natural Science Foundation of China (NFSC) under grant No. 11572327, No. 51971013, U1537212 and No. 51471019, and the Strategic Priority Research Program of Chinese Academy of Sciences under grant No. XDA17030100, and XDA17030200.

References

[1] N.P. Padture, M. Gell, E.H. Jordan, Thermal barrier coatings for gas-turbine engine applications, Science 296 (5566) (2002) 280.
[2] R.L. Jones, Thermal barrier coatings, in: K.H. Stern (Ed.), Metallurgical and Ceramic Protective Coatings, Springer Netherlands, Dordrecht, 1996, pp. 194–235.
[3] A.G. Evans, D.R. Mumm, J.W. Hutchinson, G.H. Meier, F.S. Pettit, Mechanisms controlling the durability of thermal barrier coatings, Prog. Mater. Sci. 46 (5) (2001) 505–553.
[4] D.R. Clarke, M. Oechsner, N.P. Padture, Thermal-barrier coatings for more efficient gas-turbine engines, MRS Bull. 37 (10) (2012) 891–898.
[5] K.W. Schlichting, N.P. Padture, E.H. Jordan, M. Gell, Failure modes in plasma sprayed thermal barrier coatings, Mater. Sci. Eng., A 342 (1) (2003) 120–130.
[6] W. Chi, S. Sampath, H. Wang, Microstructure-thermal conductivity relationships for plasma-sprayed yttria-stabilized zirconia coatings, J. Am. Ceram. Soc. 91 (8) (2008) 2636–2645.
[7] S.-y. Qiu, Y.-C. Liu, H.-b. Guo, C.-G. Huang, Y. Ma, C.-W. Wu, Effect of splat-interface discontinuity on effective thermal conductivity of plasma sprayed thermal barrier coating, Ceram. Int. 46 (4) (2020) 4824–4831.
[8] J. Singh, D.E. Wolfe, J. Singh, Architecture of thermal barrier coatings produced by electron beam-physical vapor deposition (EB-PVD), J. Mater. Sci. 37 (2002) 3261.
[9] J. Singh, D.E. Wolfe, R.A. Miller, J.I. Eldridge, D.M. Zhu, Tailored microstructure of zirconia and hafnia-based thermal barrier coatings with low thermal conductivity and high hemispherical reflectance by EB-PVD, J. Mater. Sci. 39 (2004) 1975–1985.
[10] S.Y. Qiu, C.W. Wu, C.G. Huang, Y. Ma, H.B. Guo, Microstructure dependence of effective thermal conductivity of EB-PVD TBCs, Materials 14 (8) (2021).
[11] H.B. Guo, R. Vaßen, D. Stöver, Thermophysical properties and thermal cycling behavior of plasma sprayed thick thermal barrier coatings, Surf. Coating. Technol. 192 (2005) 48–56.
[12] J. Wu, H.-b. Guo, L. Zhou, L. Wang, S.-k. Gong, Microstructure and thermal properties of plasma sprayed thermal barrier coatings from nanostructured YSZ, J. Therm. Spray Technol. 19 (2010) 1186–1194.
[13] J.R. Nicholls, K.J. Lawson, A. Johnstone, D.S. Rickerby, Methods to reduce the thermal conductivity of EB-PVD TBCs, Surf. Coating. Technol. 151 (2002) 383–391.
[14] H.D. Steffens, Z. Babiak, M. Gramlich, Some aspects of thick thermal barrier coating lifetime prolongation, J. Therm. Spray Technol. 8 (1999) 517–522.
[15] L. Gao, H. Guo, L. Wei, C. Li, H. Xu, Microstructure, thermal conductivity and thermal cycling behavior of thermal barrier coatings prepared by plasma spray physical vapor deposition, Surf. Coating. Technol. 276 (2015) 424–430.
[16] K. von Niessen, M. Gindrat, A. Refke, Vapor phase deposition using plasma Spray-PVD, J. Therm. Spray Technol. 19 (2010) 502–509.
[17] A. Refke, D. Hawley, J. Doesburg, R. Schmid, LPPS thin film technology for the application of TBC systems, Proc. Int. Therm. Spray Conf. (2005) 438–443.
[18] K.V. Niessen, M. Gindrat, Plasma spray-PVD: a new thermal spray process to deposit out of the vapor phase, J. Therm. Spray Technol. 20 (2011) 736–743.
[19] C. Li, H. Guo, L. Gao, L. Wei, S. Gong, H. Xu, Microstructures of yttria-stabilized zirconia coatings by plasma spray-physical vapor deposition, J. Therm. Spray Technol. 24 (3) (2014) 534–541.
[20] B. Zhang, L. Wei, H. Guo, H. Xu, Microstructures and deposition mechanisms of quasi-columnar structured yttria-stabilized zirconia coatings by plasma spray physical vapor deposition, Ceram. Int. 43 (15) (2017) 12920–12929.
[21] L. Gao, L. Wei, H. Guo, S. Gong, H. Xu, Deposition mechanisms of yttria-stabilized zirconia coatings during plasma spray physical vapor deposition, Ceram. Int. 42 (4) (2016) 5530–5536.
[22] Z.-G. Liu, J.-H. Ouyang, Y. Zhou, X.-L. Xia, Structure and thermal conductivity of Gd2(TixZr1−x)2O7 ceramics, Mater. Lett. 62 (2008) 4455–4457.
[23] S. Li, W. He, J. Shi, L. Wei, J. He, H. Guo, PS-PVD gadolinium zirconate thermal barrier coatings with columnar microstructure sprayed from sintered powder feedstocks, Surf. Coating. Technol. 383 (2020).
[24] R.-B. Zhu, J.-P. Zou, J. Mao, Z.-Q. Deng, X.-F. Zhang, C.-M. Deng, M. Liu, A comparison between novel Gd2Zr2O7 and Gd2Zr2O7/YSZ thermal barrier coatings fabricated by plasma spray-physical vapor deposition, Rare Met. 40 (8) (2020) 2244–2253.
[25] K.D. Maglic, A. Cezairliyan, V.E. Peletsky, Compendium of Thermophysical Property Measurement Methods, vol. 1, survey of measurement techniques, 1984.
[26] J. Leitner, P. Chuchvalec, D. Sedmidubský, A. Strejc, P. Abrman, Estimation of heat capacities of solid mixed oxides, Thermochim. Acta 395 (1–2) (2002) 27–46.
[27] Y.J. Liang, Y.C. Che, X.X. Liu, N.J. Li, Manual of Practical Inorganic Matter Thermodynamics, Northeastern University Press, Shenyang, 1993.
[28] L. Guo, H.B. Guo, S.K. Gong, et al., Improvement on the phase stability, mechanical properties and thermal insulation of Y_2O_3-stabilized ZrO_2 by Gd_2O_3 and Yb_2O_3 co-doping, Ceram. Int. 39 (2013) 9009–9015.
[29] F. Shao, H. Zhao, X. Zhong, Y. Zhuang, Z. Cheng, L. Wang, S. Tao, Characteristics of thick columnar YSZ coatings fabricated by plasma spray-physical vapor deposition, J. Eur. Ceram. Soc. 38 (4) (2018) 1930–1937.
[30] M. Mantyla, Boolean operations of 2-manifolds through vertex neighborhood classification [J], Acm T Graphic 5 (1) (1986) 1–29.
[31] Scott Roth, Ray casting for modeling solids[J], Comput. Graph. Image Process. 18 (2) (1981) 109–144.
[32] P.J. Schneider, D.H. Eberly, Chapter 11 - intersection IN 3D, in: P.J. Schneider, D. H. Eberly (Eds.), Geometric Tools for Computer Graphics, Morgan Kaufmann, San Francisco, 2003, pp. 481–662.
[33] L. Guo, H. Guo, H. Peng, S. Gong, Thermophysical properties of Yb2O3 doped Gd2Zr2O7 and thermal cycling durability of (Gd0.9Yb0.1)2Zr2O7/YSZ thermal barrier coatings, J. Eur. Ceram. Soc. 34 (5) (2014) 1255–1263.
[34] D. Zhou, D.E. Mack, E. Bakan, G. Mauer, D. Sebold, O. Guillon, R. Vaßen, Thermal cycling performances of multilayered yttria-stabilized zirconia/gadolinium zirconate thermal barrier coatings, J. Am. Ceram. Soc. 103 (3) (2019) 2048–2061.
[35] S. Mahade, N. Curry, S. Björklund, N. Markocsan, P. Nylén, Thermal conductivity and thermal cyclic fatigue of multilayered Gd2Zr2O7/YSZ thermal barrier coatings processed by suspension plasma spray, Surf. Coating. Technol. 283 (2015) 329–336.
[36] S. Mahade, N. Curry, K.P. Jonnalagadda, R.L. Peng, N. Markocsan, P. Nylén, Influence of YSZ layer thickness on the durability of gadolinium zirconate/YSZ double-layered thermal barrier coatings produced by suspension plasma spray, Surf. Coating. Technol. 357 (2019) 456–465.